This is an open access article published under a Creative Commons Attribution (CC-BY) License, which permits unrestricted use, distribution and reproduction in any medium, provided the author and source are cited.

THE JOURNAL OF PHYSICAL CHEMISTRY C

Article

pubs.acs.org/JPCC

Density Functional Theory Study of the Adsorption of Hydrazine on the Perfect and Defective Copper (100), (110), and (111) Surfaces

Saeedeh S. Tafreshi, Alberto Roldan, and Nora H. de Leeuw*

Department of Chemistry, University College London, 20 Gordon Street, London WC1H 0AJ, United Kingdom

ABSTRACT: We have calculated the adsorption of the reducing agent hydrazine (N_2H_4) on copper surfaces using density functional theory calculations with a correction for the long-range interactions (DFT-D2). We have modeled the perfect and a number of defective Cu(100), (110), and (111) surfaces, which are found in the experimentally produced structures of copper nanoparticles. We have studied adsorption of hydrazine at three types of defects in the surfaces, i.e., monatomic steps, Cu adatoms, and Cu vacancies. Several low-energy adsorption structures for hydrazine on each perfect and defective surface have been identified and compared. Our calculations reveal that hydrazine bridges surface copper atoms, with the molecule twisted from the gauche toward an eclipsed conformation, except on the adatom (100) and vacancy-containing (100) and (110) surfaces, where it adsorbs through one nitrogen atom in gauche and trans conformations, respectively. The strongest adsorption energy is found on the stepped (110) surface, where hydrazine bridges between the copper atoms on the step edge and the terrace, as it stabilizes the low-coordinated copper atoms. Our results show that, although the (110) surface contains a number of low-coordinated atoms that enhance the surface-molecule interactions, the addition of defects on the more stable (111) and (100) surfaces provides sites that enable hydrazine binding to almost the same extent. This study also confirms general observations of surface adsorption trends in terms of d-band center and binding energy as a function of coordination number, i.e., the stronger the molecular adsorption, the higher the d-band shifts at low-coordinated sites.

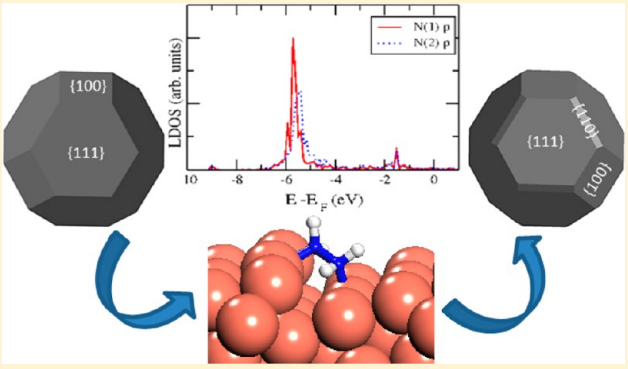

1. INTRODUCTION

Over the last two decades, nanoparticles smaller than 100 nm have received much attention due to their applications in a wide range of areas,[1] including catalysis, magnetics, optoelectronics, electronic materials, biological identification, labeling, environmental detection, and monitoring.[2−4] This wide applicability is in part due to their position between isolated atoms and extended solids as well as their surface properties, since they are composed almost entirely of surfaces. The formation of copper nanoparticles with specific properties, which are influenced by their shape, size, and structure,[5−10] is of interest in the design of materials for particular applications.

Generating specific nanoparticles with defined morphologies depends on several parameters such as bulk solvent type, temperature, pressure, and synthesis devices. One particular factor during synthesis, which experiment has shown results in significant changes in the distribution of copper particle shapes and sizes, is the variation in the concentration of reducing agents like hydrazine (N_2H_4).[11,12] Although experimental work, e.g., in reverse micelle-based synthesis, has achieved much in the way of controlling the size and shape of copper nanoparticles,[13] the underlying processes are still not fully understood, and molecular-level information would help to generate tailored particles more efficiently.

More generally, N_2H_4 itself has applications in fuel cells, for example in direct hydrazine fuel cells using proton exchange membranes and room-temperature hydrazine/air direct-liquid fuel cells based on the use of nanostructured copper electrodes.[14−16] The copper-hydrazine interface is thus of importance in a number of applications, and in order to produce copper particles with specific properties or improve copper electrodes for more efficient fuel cells, we need to gain fundamental understanding of the interactions between N_2H_4 and Cu surfaces.

Computational techniques based on the density functional theory (DFT) have become an important tool for unravelling the interactions between adsorbates and surfaces. We have employed them in earlier works to improve our understanding of copper nanoparticle production methods by investigating surface processes occurring at the molecular level.[17−21] Following our investigation of the adsorption of molecular hydrazine on dominant Cu(111) surfaces,[21] we have now carried out first-principles calculations of the interaction of N_2H_4 with the Cu(100) and (110) surfaces, which are also found experimentally. Compared to the (111), where hydrazine prefers to adsorb through both nitrogen atoms with a rotation around the N−N bond from a gauche toward an eclipsed conformer, different surface geometries such as less close-packed atomic arrange-

Received: August 4, 2014
Revised: October 14, 2014
Published: October 15, 2014

 © 2014 American Chemical Society dx.doi.org/10.1021/jp5078664 | J. Phys. Chem. C 2014, 118, 26103−26114

ments, low-coordinated surface atoms and longer Cu−Cu distances, may modify the way the molecule is accommodated at the copper surface.

To obtain an atomistic understanding of the N_2H_4 interaction with realistic surface structures, we have studied three types of surface defects: surface steps, where the copper terraces are offset by one atomic layer from plane to plane, Cu adatoms, and Cu vacancies. Low-coordinated atoms provide sites for stronger adsorption, especially to those molecules that have lone-pair electrons,[22] which is shown by larger adsorption energies and shorter distances for the adsorbates bound at those sites.

2. COMPUTATIONAL METHODS

Density functional theory (DFT-D2) calculations including the long-range dispersion correction approach by Grimme[23,24] were employed to simulate the copper bulk and surface structures as well as the hydrazine adsorption. We have used the Vienna ab-initio simulation package (VASP),[25−28] with the projector augmented wave (PAW) potentials and the generalized gradient approximation (GGA) based on the Perdew−Burke−Ernzerhof (PBE) exchange-correlation functional.[29−31] We have used the global scaling factor optimized for PBE ($s_6 = 0.75$) and a damping function to avoid near singularities for small distances; the total energy is therefore calculated as a function of the dispersion coefficient for each atom pair. The geometries of all stationary points were found with the conjugate gradient algorithm and considered converged when the force on each ion dropped below 0.01 eV/Å, whereas the energy threshold-defining self-consistency of the electron density was set to 10^{-5} eV. The valence orbitals are calculated as linear combinations of plane waves, and the size of the basis set is determined by a cutoff energy of 600 eV, whereas the core electrons are kept frozen during the calculations. Calculations were carried out using Monkhorst−Pack[32] grids of 11 × 11 × 11 k-points for the bulk simulation. We obtained a lattice parameter of 3.571 Å from the bulk optimization of the fcc metal with an error of ∼1.2% compared to the experimental value of 3.614 Å.[33] The perfect, adatom and vacancy surfaces were modeled by four-layer slabs and each full simulation cell was grown into a 2 × 2 supercell for the (100) surface, with a 5 × 5 × 1 k-point grid, and a 3 × 2 supercell for the (110) surface, with a 3 × 5 × 1 k-point grid. The surface areas then correspond to a hydrazine coverage (θ_{N2H4}) of 0.125 and 0.083 ML on the (100) and (110) respectively, where ML is defined as the number of molecules divided by the number of Cu atoms at the surface. At these coverages, the closest NH_2−NH_2 distances for neighboring hydrazine molecules are 5.91 and 8.84 Å on the (100) and (110), respectively, precluding lateral interactions between molecules in adjacent unit cells. During the geometry optimizations, we allowed the adsorbate molecule and three top surface layers to relax, while the rest of the atoms in the slab were fixed at their bulk lattice positions. The stepped surfaces were modeled by a 3 × 2 supercell of two frozen layers and four free layers of Cu atoms, giving a θ_{N2H4} of 0.083 ML, and using a 3 × 5 × 1 k-point grid. On the stepped surfaces, the hydrazine molecules are not interacting with their images in neighboring cells either, as the shortest NH_2−NH_2 distances are 7.44 and 7.05 Å on the (100) and (110), respectively. This setup, where one side of the slab is kept fixed, ensures the explicit geometry optimization of a realistic number of surface layers, while still retaining a reasonably sized slab, which made it feasible to investigate a large number of initial adsorption geometries. A vacuum of 20 Å was introduced between the slabs and their periodic images to avoid perpendicular interactions.

To characterize the surface stabilities of the various Cu surfaces, we have computed the surface energy (γ) which is a measure of the thermodynamic stability of a given surface; the smaller its value, the more stable the surface. We have calculated the relaxed surface energy (γ_r) using eq 1, where $E_{slab,r}$ is the energy of the relaxed slab with one side fixed in the optimized bulk geometry, $E_{slab}^{unrelaxed}$ is the total energy of the unrelaxed slab prior to surface geometry optimization, E_{bulk} is the energy of the primitive cell containing one Cu atom, n is the number of atoms in the slab, and A is the surface area of one side of the slab.

$$\gamma_r = \frac{E_{slab,r} - nE_{bulk}}{A} - \frac{E_{slab}^{unrelaxed} - nE_{bulk}}{2A} \quad (1)$$

The formation energy of a defect is the amount of energy required to create it. We have calculated the vacancy and adatom formation energies using eqs 2 and 3, respectively

$$E_{f,vac} = (E_{vac,r} + E_{bulk}) - E_{perfect,r} \quad (2)$$

$$E_{f,adatom} = E_{adatom,r} - (E_{bulk} + E_{perfect,r}) \quad (3)$$

where $E_{vac,r}$ and $E_{adatom,r}$ are the total energies of the relaxed slab with one side fixed in the optimized bulk geometry, containing a vacancy and adatom at the relaxed site of the slab, respectively, and $E_{perfect,r}$ is the energy of the relaxed defect-free surface with one side fixed in the optimized bulk geometry.

We have optimized the three major conformations of hydrazine in the gas phase: gauche, trans, and eclipsed, see Figure 1. The gauche conformer is the lowest-energy structure,

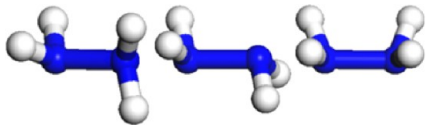

Figure 1. Representation of the N_2H_4 conformations, from left to right: gauche, trans, and eclipsed.

with the trans and eclipsed conformations being 0.13 and 0.36 eV higher in energy, respectively. We started our investigation by placing the different conformers in a number of initial configurations at a variety of positions on the perfect and defective Cu (100) and (110) surfaces in order to identify the lowest-energy systems. Although the copper surfaces do not contain intrinsic dipoles, adsorption of the hydrazine molecule on one side of the slab gives rise to a dipole perpendicular to the surface and we have therefore employed the dipole correction in VASP to aid convergence.

The adsorption energy (E_{ads}) was calculated as the difference between the total energy of the optimized substrate−adsorbate system ($E_{slab+N_2H_4}$) and the sum of the relaxed clean surface (E_{slab}) and isolated N_2H_4 in the gauche conformation ($E_{N_2H_4}$), eq 4

$$E_{ads} = E_{slab+N_2H_4} - (E_{slab} + E_{N_2H_4}) \quad (4)$$

3. RESULTS AND DISCUSSION

3.1. Surface Properties. We have first created the perfect Cu(100), (110), and (111) surfaces (Figure 2). The (100) surface is a square lattice obtained by cleaving the face-centered bulk plane with a Cu−Cu distance of 2.52 Å (Figure 2a), while the (110) surface has a rectangular lattice and atoms are aligned with a distance of 2.52 Å between Cu atoms and distance of 3.57 Å between elevated rows (Figure 2b). The (111) surface is the

dx.doi.org/10.1021/jp5078664 | J. Phys. Chem. C 2014, 118, 26103−26114

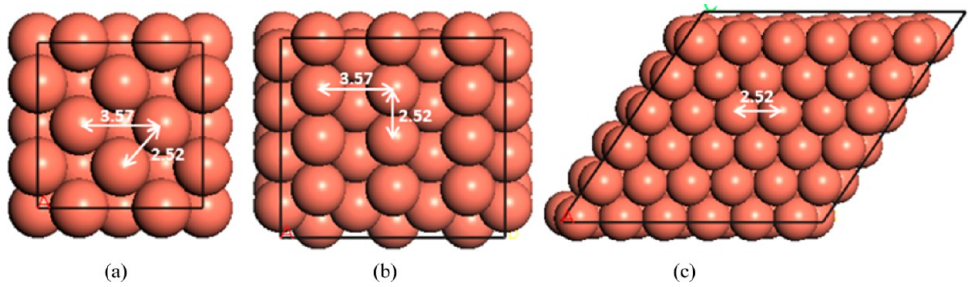

Figure 2. Surface structures (top-view) of the perfect (a) Cu(100), (b) Cu(110) and (c) Cu(111), the last one added for comparison.[21] Black frames limit the cell used in the calculations while arrows indicate distances in Å.

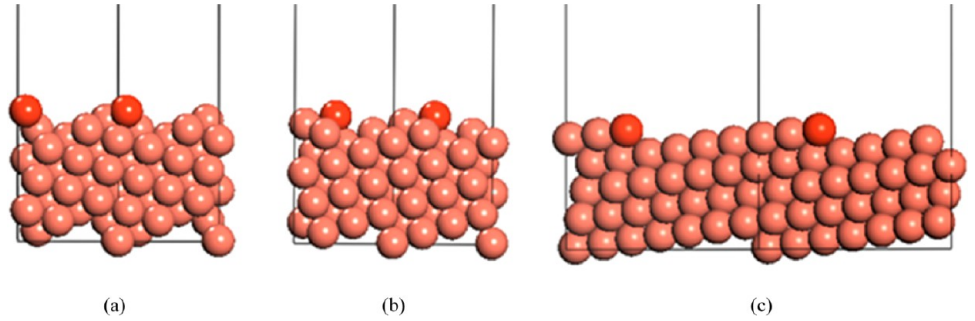

Figure 3. Side view of simulation cells used in the calculations of stepped surfaces where the low-coordinated copper atoms are shaded darker: (a) Cu(100), (b) Cu(110), and (c) Cu(111) for comparison.[21]

hexagonal close-packed surface with Cu−Cu distances of 2.52 Å (Figure 2c).

However, as experimental surface structures are never perfect, we have also created three defects on the surfaces: steps, adatoms and vacancies.

The stepped surfaces have been studied to investigate the presence of an extended edge of low-coordinated atoms on the surface stabilities and adsorption behavior. Each unit cell (shown in Figure 3a−c) in the stepped slab was offset by one atomic layer with respect to the next cell.[34−36]

One point defect on the surface that we have investigated is a Cu atom added at different sites of the relaxed side of the slab (Figure 4a−c). As Figure 4 shows, we have studied three different

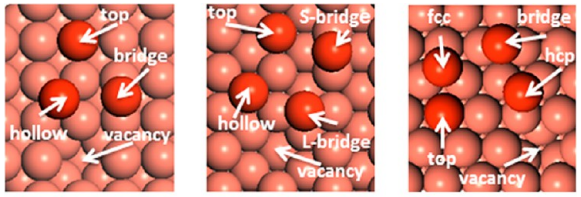

Figure 4. Surface geometry (top-view) of different adatom sites for (a) (100) and (b) (110) as well as (c) (111) surfaces for comparison.[21] Copper adatoms are shaded darker. A vacancy defect on each surface is also shown. S-bridge and L-bridge indicate the short and long bridges sites on the (110) surface, respectively.

adatom adsorption sites: hollow, bridge, and top sites. During relaxation of the top and bridge adatom, we restricted its movement, allowing perpendicular movement to the surface only to keep it at these lateral positions. These calculations enabled us to obtain energies for these higher energy adatom positions, which could provide information on pathways for adatom diffusion across the copper surface.[37,38] Because of the uneven structure of the (110) surface, adatoms can bridge two different sites on the rows: between two copper surface atoms along either long or short edge, which are separated by 3.57 Å (long-bridge) or 2.52 Å (short-bridge), respectively (Figure 4b). Finally, we have studied a surface vacancy, where one of the atoms in the top layer has been removed from the slab, also shown in Figure 4a−c.

As shown by the formation energies in Table 1, the hollow site is the preferred place for the adatom on the Cu surfaces with

Table 1. Formation Energies of Cu-Adatom and Vacancy on the Cu(100), (110), and (111) Surfaces

surface site	E_f (eV), (100)	E_f (eV), (110)	E_f (eV), (111)[21]
hollow	0.54, 0.66,[39] 0.71[38]	0.30, 0.31,[39] 0.31[38]	0.83 (fcc), 0.85 (hcp), 0.93,[39] 0.97[38]
bridge	1.01	0.50 (l-bridge), 1.37 (s-bridge)	1.01
top	1.37	1.68	1.19
vacancy	0.48, 0.58[39]	0.35, 0.29[39]	0.82, 0.72[39]

formation energies of 0.54 and 0.30 eV on the (100) and (110) surfaces, respectively, less endothermic than on the (111) surface.[21] Although formation of a vacancy is energetically less expensive than that of an adatom on the (100) by 0.06 eV, but less favorable on the (110) by 0.05 eV, both are more likely to form than on the (111). This is due to the higher relative stability of the (111) surface and lower coordination to the adatom on the (111) than on the (100) and (110). Our results are in agreement with previous reports,[38,39] where the adatom-hollow and vacancy formation energies on the (111) were larger than those on (100) and (110) surfaces.

Table 2 summarizes the calculated surface energies of the low-index perfect and defective copper surfaces. These surfaces show stabilities increasing from (110) < (100) < (111). As expected, the presence of defects affects the stabilities of the planes and the

dx.doi.org/10.1021/jp5078664 | J. Phys. Chem. C 2014, 118, 26103−26114

Table 2. Surface Energies of the Perfect and Defective (100) and (110) Copper Surfaces[a]

surface	$\gamma_{(100)}$ (J m^{-2})	$\gamma_{(110)}$ (J m^{-2})	$\gamma_{(111)}$ (J m^{-2})[21]
perfect	2.08, 2.09,[40] 2.166[41]	2.14, 2.31,[40] 2.237[41]	1.97, 1.96,[40] 1.952[41]
stepped	2.45	2.58	2.10
adatom (hollow)	2.23	2.19	2.04
adatom (bridge)	2.37	2.22 (l-bridge), 2.34 (s-bridge)	2.05
adatom (top)	2.48	2.39	2.06
vacant	2.21	2.19	2.04

[a]The surface energies of (111) are also reported for comparison.

trend changes to (100) < (110) for the adatom and vacancies, although the (111) remains the most stable surface in all cases. The small discrepancies between our results and previous theoretical studies reported in Table 2 are due to the variation in methods used.

3.2. N_2H_4 Adsorption on the Cu(111) Surfaces. We have already investigated hydrazine adsorption on the perfect and defective Cu(111) surfaces[21] but summarize our findings here for ease of comparison. Figures 5a–d show the most favorable

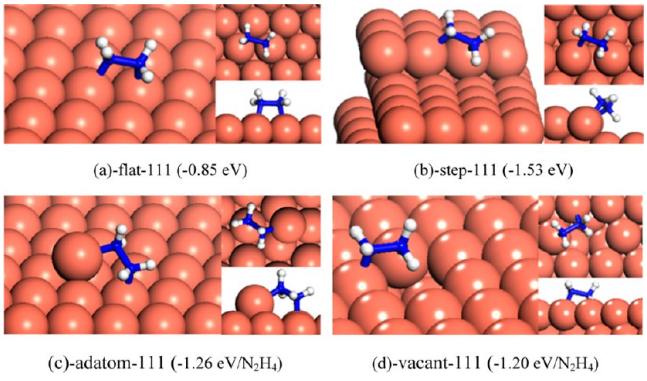

Figure 5. Surface geometry of the lowest-energy configurations for adsorption of N_2H_4 on the (a) flat, (b) step, (c) adatom, and (d) vacant Cu(111) surfaces. (Adsorption energies are given in parentheses.[21])

adsorption structures on the Cu(111) showing that hydrazine prefers to adsorb through both nitrogen atoms to perfect and defective surfaces. The stepped surface is the least stable, and hence more reactive, of the (111) planes leading to the highest adsorption energy with the hydrazine bridging across the step edge.

3.3. N_2H_4 Adsorption on the Cu(100) Surfaces. *3.3.1. Adsorption on the Perfect (100) Surface.* The lowest-energy structures for hydrazine adsorption on the perfect (100) surface are represented in Figure 6, with structural and energetic details listed in Table 3.

Table 3. Geometries and Adsorption Energies (E_{ads}) of the Relaxed N_2H_4 Adsorbed Structures on the Perfect Cu(100) Surface[a]

label	geometry	E_{ads} (eV/N_2H_4)	N–Cu (Å)	N–Cu (Å)	N–N (Å)	Θ (deg)
flat-100a	bridge	−1.17	2.12	2.12	1.45	0.20
flat-100b	trans	−1.07	2.06	**3.05**	1.48	23.77
flat-100c	gauche	−1.07	2.09	**3.01**	1.45	26.75

[a]The angle between the N–N bond and the surface plane is Θ, the N–N bond length in the gas phase is 1.44 Å. Bold numbers indicate a nonbonding nitrogen atom.

In the most favorable configuration, the hydrazine molecule lies parallel to the surface, having rotated around the N–N bond toward the eclipsed conformer. It binds to the surface through both nitrogen atoms with Cu–N distances of 2.12 Å and releasing an adsorption energy of E_{ads} = −1.17 eV/N_2H_4 (Figure 6, flat-100a). Although the adsorption structure is similar to the one on the (111),[21] the molecule adsorbs more strongly to the (100) by 0.32 eV/N_2H_4. In the most favorable structure for the adsorption of hydrazine on the perfect Cu(100) identified by Daff et al. using pure DFT,[17] the molecule was in the gauche conformation and bound to only one Cu surface atom, releasing an adsorption energy of 0.57 eV/N_2H_4 which is only half of our calculated adsorption energy, showing the importance of including the dispersion correction in DFT calculations of this type of systems.

The next two favored structures were obtained from hydrazine in the trans and gauche conformations, aligned perpendicularly to the plane and placed atop a copper atom (Figure 6, flat-100b, c). Despite producing the same adsorption energies, the trans conformer is bound to the surface with a slightly shorter Cu–N distance of 2.06 Å compared to 2.09 Å for the gauche conformer.

3.3.2. Adsorption on the Stepped (100) Surface. Figure 7 and Table 4 show the properties of the three lowest-energy adsorption structures on the stepped Cu(100) surface. We found two adsorption configurations, where the hydrazine adsorbs in the gauche configuration on the step atoms, both releasing the same adsorption energy (−1.29 eV/N_2H_4) (Figure 7, step-100a, b) which is, however, weaker by 0.24 eV/N_2H_4 than observed on the (111) surface.[21]

A third configuration is found from an initial structure with the hydrazine in the gauche conformer aligned perpendicularly to the plane. Upon optimization, the molecule adsorbs with one N on top of a terrace Cu atom (Figure 7, step-100c), releasing an energy of 1.17 eV/N_2H_4.

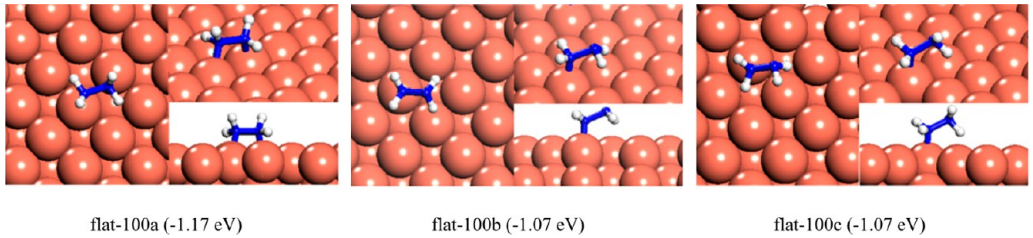

Figure 6. Surface geometries of the lowest-energy configurations for adsorption of N_2H_4 on the perfect Cu(100) surface. (Adsorption energies are given in parentheses.)

dx.doi.org/10.1021/jp5078664 | J. Phys. Chem. C 2014, 118, 26103–26114

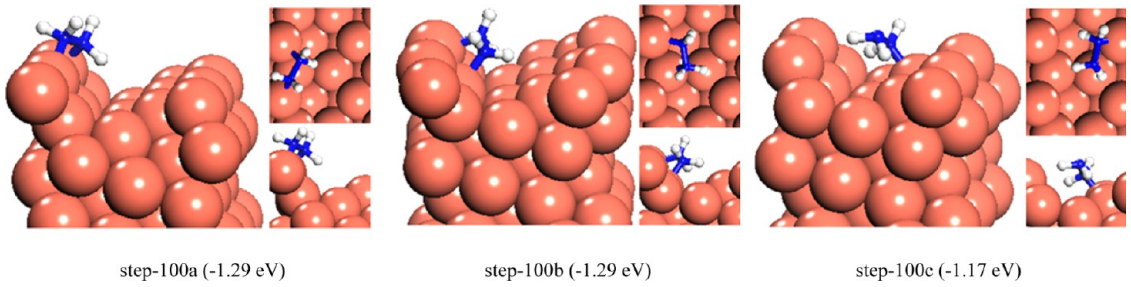

Figure 7. Lowest-energy configurations for adsorption of N_2H_4 on the stepped Cu(100) surface. (Adsorption energies are given in parentheses.)

Table 4. Geometries and Adsorption Energies (E_{ads}) of the Relaxed N_2H_4 Adsorbed Structures on the Stepped Cu(100) Surface[a]

label	geometry	E_{ads} (eV/N_2H_4)	N−Cu (Å)	N−Cu (Å)	N−N (Å)	Θ (deg)
step-100a	bridge-step	−1.29	2.12	2.12	1.46	15.73
step-100b	bridge-step	−1.29	2.10	2.16	1.45	11.93
step-100c	gauche-atop-terrace	−1.17	2.08	**3.04**	1.45	28.08
step-100d	bridge-terrace	−1.14	2.11	2.20	1.45	8.07
step-100e	gauche-atop-step	−1.06	2.04	**2.94**	1.45	35.21
step-100f	trans-atop-terrace	−1.05	2.05	**2.98**	1.47	40.73
step-100g	gauche-atop-terrace	−1.05	2.08	**2.96**	1.44	38.57

[a]Bold numbers indicate a nonbonding nitrogen atom.

We found a number of weaker adsorption structures (step-100d-g) which are summarized in Table 4.

When the molecule adsorbed atop of a Cu atom on the step edge (step-100e), it is less strongly bound by 0.11 eV/N_2H_4 than when it is located atop a copper atom on the terrace (step-100c), in contrast to the results for the (111) surface.[21] As the (100) surface is already relatively unstable itself, the step edges on this surface are not necessarily more reactive than the terrace.

3.3.3. Adsorption on the (100) Adatom Surface. As Table 2 shows, the hollow-adatom Cu(100) surface provides the most stable adatom site on the surface, and we have therefore investigated adsorption of hydrazine on this surface from a number of different starting configurations. The lowest-energy adsorption structures are shown in Figure 8 with the adsorption geometries and energetics listed in Table 5.

The most stable geometry is obtained with hydrazine in the gauche conformation, with one nitrogen atom at a position slightly displaced from the top site of the Cu-adatom (Figure 8, adatom-100a) and the N−N bond almost parallel to the surface. This adsorption releases 1.18 eV/N_2H_4, the same amount when the molecule binds to the surface Cu atoms nearby the adatom (Figure 8, adatom-100b), where hydrazine is lying flat with a torsion of 31.68° from the gauche conformation toward the eclipsed conformer. This adsorption structure is similar to that of the molecule bridging in gauche conformation to the perfect (100) surface, releasing very similar binding energies. This result is in contrast to the (111) surface,[21] where the adsorption on the adatom is stronger and it shows that the introduction of an adatom on the (100) surface does not have as prominent an effect on the hydrazine adsorption as on the (111). The most favorable adsorption structure on the adatom (100) calculated using pure DFT[18] resulted in a much smaller adsorption energy of −0.97 eV/N_2H_4 and in this configuration hydrazine binds with one nitrogen on top of the adatom.

Figure 8 shows both adatom-100c and adatom-100d configurations where hydrazine binds to the adatom on the surface. While hydrazine in adatom-100d is bound more closely to the copper atoms (N−Cu distance of 2.13 Å), with a rotation of 22.6° from the gauche conformation, the adatom-100c (N−Cu distance of 2.19 Å) is energetically more favorable, being only rotated 3.5° toward the eclipsed conformer. Hydrazine also

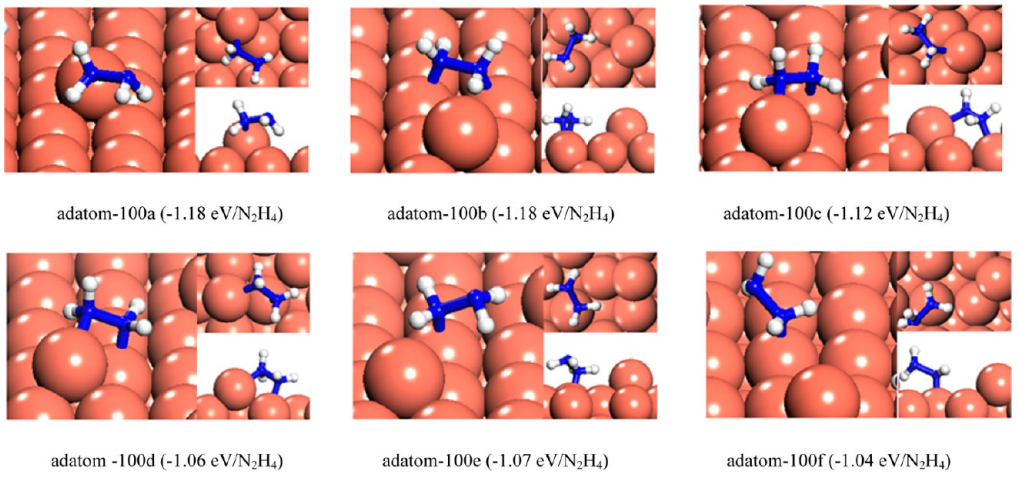

Figure 8. Surface geometry of the lowest-energy configurations for adsorption of N_2H_4 on the adatom Cu(100) surface. (Adsorption energies are given in parentheses.)

dx.doi.org/10.1021/jp5078664 | J. Phys. Chem. C 2014, 118, 26103−26114

Table 5. Geometries and Adsorption Energies (E_{ads}) of the Relaxed N_2H_4 Adsorbed Structures on the Adatom Cu(100) Surface[a]

label	geometry	E_{ads} (eV/N_2H_4)	N−Cu (Å)	N−Cu (Å)	N−N (Å)	Θ (deg)
adatom-100a	gauche-atop-adatom	−1.18	**2.07**	3.01	1.46	8.15
adatom-100b	bridge-surface atoms	−1.18	2.10	2.11	1.45	0.20
adatom-100c	bridge-adatom-surface atom	−1.12	**2.19**	2.19	1.46	16.75
adatom-100d	bridge-adatom-surface atom	−1.06	**2.13**	2.15	1.45	25.6
adatom-100e	trans-atop-surface atom	−1.07	2.05	3.02	1.41	27.42
adatom-100f	gauche-atop-surface atom	−1.04	2.08	3.02	1.45	24.81

[a]Bold numbers indicate a nitrogen atom is bound to the adatom.

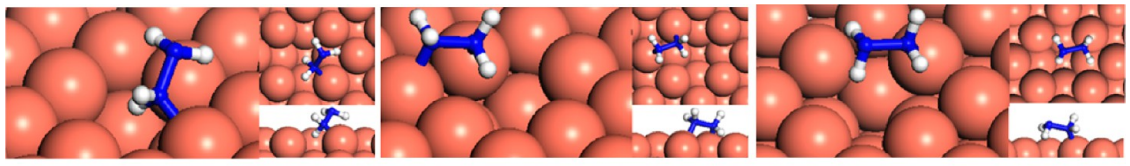

vacant-100a (-1.23 eV/N_2H_4) vacant-100b (-1.19 eV/N_2H_4) vacant-100c (-1.15 eV/N_2H_4)

Figure 9. Lowest-energy configurations for adsorption of N_2H_4 on the Cu(100) vacancy surface. (Adsorption energies are given in parentheses.)

adsorbs atop the surface copper atom through only one nitrogen atom, without bridging, in either trans or gauche conformer (adatom-100e, f).

3.3.4. Adsorption on the (100) Vacancy Surface. Finally, we have investigated the adsorption of N_2H_4 at Cu vacancies on the (100) surface. The lowest-energy structures are schematically shown in Figure 9, with geometric and energetic details summarized in Table 6. In the strongest adsorption configuration, releasing an energy of 1.23 eV/N_2H_4, the molecule in the gauche conformation interacts through only one nitrogen with the surface Cu next to the vacancy, with a Cu−N distance of 2.07 Å, and inclined to the surface by an angle of 41.53° (Figure 9, vacant-100a). The adsorption structure of hydrazine bridging two Cu atoms next to the vacancy, with an adsorption energy of −1.19 eV/N_2H_4 (Figure 9, vacant-100b), is weaker than the vacant-100a configuration but comparable to the same structure on the Cu(111) surface.[21] A local minimum was found for the molecule adsorbed in the trans conformation on top of the atom next to the vacancy (Figure 9, vacant-100c), releasing an adsorption energy of 1.15 eV/N_2H_4.

Table 6. Geometries and Adsorption Energies (E_{ads}) of the Relaxed N_2H_4 Adsorbed Structures on the Cu(100) Vacancy Surface[a]

label	geometry	E_{ads} (eV/N_2H_4)	N−Cu (Å)	N−Cu (Å)	N−N (Å)	Θ (deg)
vacant-100a	gauche-atop	−1.23	2.07	**3.06**	1.45	41.53
vacant-100b	bridge	−1.19	2.07	2.14	1.45	12.21
vacant-100c	trans-atop	−1.15	2.05	**3.04**	1.47	11.24

[a]Bold numbers indicate a nonbonding nitrogen atom.

3.4. N_2H_4 Adsorption on the Cu(110) Surfaces. *3.4.1. Adsorption on the Perfect (110) Surface.* Figure 10 and Table 7 show the lowest-energy adsorption structures on the perfect Cu(110) surface. The strongest adsorption of all our calculations of the perfect (111), (100), and (110) surfaces occurred on the (110), releasing an adsorption energy of 1.34 eV/N_2H_4 (Figure 10, flat-110a). This structure has the N_2H_4 molecule lying along the short-bridge row, with Cu−N distances of 2.10 Å, in a conformation close to the gauche conformer with a torsion of about 22.5° toward the eclipsed conformation. In the

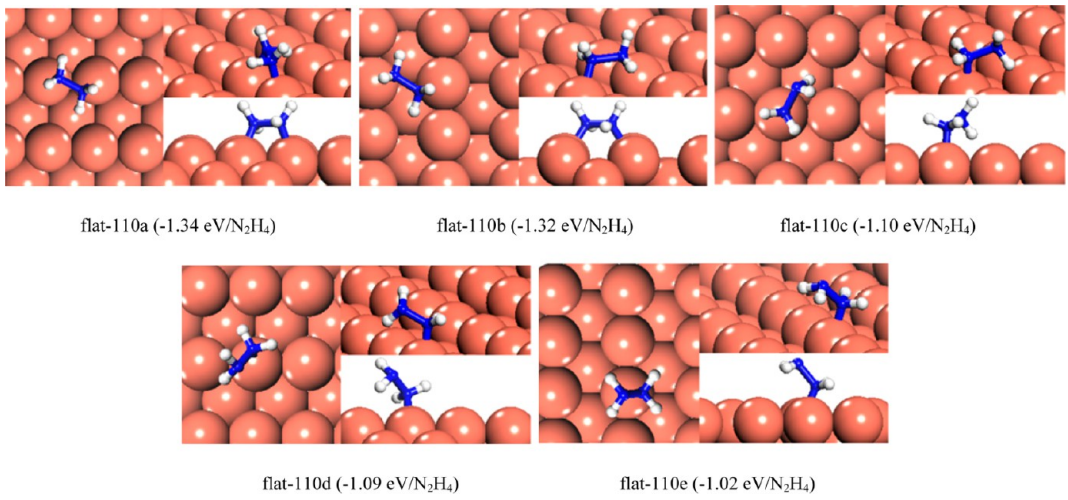

flat-110a (-1.34 eV/N_2H_4) flat-110b (-1.32 eV/N_2H_4) flat-110c (-1.10 eV/N_2H_4)

flat-110d (-1.09 eV/N_2H_4) flat-110e (-1.02 eV/N_2H_4)

Figure 10. Lowest-energy configurations for adsorption of N_2H_4 on the perfect Cu(110) surface. (Adsorption energies are given in parentheses.)

dx.doi.org/10.1021/jp5078664 | J. Phys. Chem. C 2014, 118, 26103−26114

Table 7. Geometries and Adsorption Energies (E_{ads}) of the Relaxed N_2H_4 Adsorbed Structures on the Perfect Cu(110) Surface[a]

label	geometry	E_{ads} (eV/N_2H_4)	N−Cu (Å)	N−Cu (Å)	N−N (Å)	Θ (deg)
flat-110a	bridge	−1.34	2.10	2.10	1.45	0.20
flat-110b	bridge	−1.32	2.15	2.15	1.45	0.20
flat-110c	gauche	−1.10	2.06	**2.95**	1.45	18.75
flat-110d	gauche	−1.09	2.05	**2.97**	1.45	39.94
flat-110e	trans	−1.02	2.03	**3.04**	1.41	50.96

[a]Bold numbers indicate a nonbonding nitrogen atom.

Table 8. Geometries and Adsorption Energies (E_{ads}) of the Relaxed N_2H_4 Adsorbed Structures on the Stepped Cu(110) Surface[a]

label	geometry	E_{ads} (eV/N_2H_4)	N−Cu (Å)	N−Cu (Å)	N−N (Å)	Θ (deg)
step-110a	bridge-step-terrace	−1.60	2.04	2.07	1.46	52.06
step-110b	bridge-step	−1.58	2.06	2.08	1.47	29.87
step-110c	bridge-terrace	−1.31	2.08	2.09	1.45	3.56
step-110d	bridge-terrace	−1.28	2.11	2.13	1.45	4.66
step-110e	bridge-terrace	−1.27	2.08	2.10	1.45	2.35
step-110f	bridge-terrace	−1.26	2.10	2.13	1.45	2.44
step-110g	gauche-atop-step	−1.18	2.02	**2.92**	1.45	20.56
step-110h	gauche-atop-terrace	−1.07	2.06	**2.96**	1.45	23.39
step-110i	trans-atop-terrace	−0.97	2.03	**2.97**	1.48	34.05

[a]Bold numbers indicate a nonbonding nitrogen atom.

most favorable adsorption geometry on the perfect (110), obtained using pure DFT, the hydrazine binds to the surface through both nitrogen atoms along the short-bridge row, releasing a smaller energy of 0.82 eV/N_2H_4.[17]

The geometry with N_2H_4 along a long-bridge (Figure 10, flat-110b) is less stable, but the hydrazine still binds more strongly than on either the Cu(111)[21] or (100) surfaces. The molecule remains parallel to the surface with a Cu−N distance of 2.15 Å, releasing an adsorption energy of 1.32 eV/N_2H_4. The optimization from a structure with N_2H_4 bridging two copper atoms across the diagonal of the rectangular lattice of the (110) yields a configuration with a single copper interaction, with an adsorption energy of −1.10 eV/N_2H_4 and the molecule in the gauche conformation (Figure 10, flat-110c). We also found two weaker nonbridging adsorption structures, shown in Figure 10, flat-110d and e. The optimized structures from a perpendicular hydrazine in gauche and trans conformations release energies of 1.09 and 1.02 eV/N_2H_4, respectively, with the molecule remaining in its gauche or trans conformation, whereas the nitrogen is slightly displaced from the atop position on the copper atom.

3.4.2. Adsorption on the Stepped (110) Surface. The representative lowest-energy structures for the N_2H_4 adsorption on the stepped (110) surface are shown in Figure 11 with structural and energetics details listed in Table 8.

We found the strongest adsorption on the stepped Cu(110) when N_2H_4 bridges between two copper atoms, one on the step and another on the terrace, with an adsorption energy of −1.60 eV/N_2H_4 (Figure 11-step-110a) and Cu−N distances of 2.04 and 2.07 Å. The channels between rows of atoms accommodate the hydrogen atoms much better, resulting in a torsional rotation of only 3.5° around the N−N bond toward the eclipsed conformation. The combination of these effects, and the lower coordination of the uppermost surface atoms on the stepped Cu(110) surface, results in the strongest adsorption found on any atomic step on the copper surfaces.

Bridging along the step edge is the second most favorable adsorption structure with adsorption energy of −1.58 eV/N_2H_4 (Figure 11-step-110b). The bridging configurations near the step (e.g., step-110c) are less stable with varying adsorption energies, depending either on how far the molecule is located from the step edge or in which direction it bridges. The adsorption becomes more endothermic as N_2H_4 moves away from the step edge or if the N_2H_4 geometry is stretched on the long-bridge. Adsorption of hydrazine through only one nitrogen atom leads to weaker binding to the surface.

3.4.3. Adsorption on the (110) Adatom Surface. We have studied adsorption of hydrazine in a number of different positions on the 4-fold hollow-adatom (110) surface, which, as shown in Table 2, is the most stable adatom position on the (110) surface. We found the strongest adsorption when the molecule bridges only surface atoms, stronger even than adsorption involving the adatom (Figure 12, adatom-110a). This strong binding is due to the space between rows of Cu atoms, which allows a favorable adsorption geometry with an adsorption energy of −1.40 eV/N_2H_4. When the molecule bridges along the long-bridge (Figure 12, adatom-110b), the Cu−N distances are lengthened to 2.13 and 2.17 Å, and this configuration releases an adsorption energy of 1.28 eV/N_2H_4. Pure DFT identifies the same structure as the most favorable adsorption conformation for hydrazine adsorption on the adatom (110) surface, but with weaker binding and a smaller adsorption energy of −1.11 eV/N_2H_4.[18]

As shown in Table 9, similar to the adsorption on the (100) surface, bridging from the adatom to a surface atom remote from

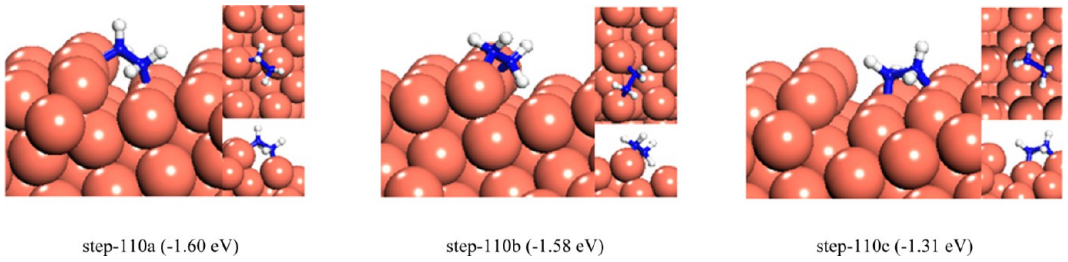

Figure 11. Lowest-energy configurations of adsorption of N_2H_4 on the stepped Cu(110) surface. (Adsorption energies are given in parentheses.)

dx.doi.org/10.1021/jp5078664 | J. Phys. Chem. C 2014, 118, 26103−26114

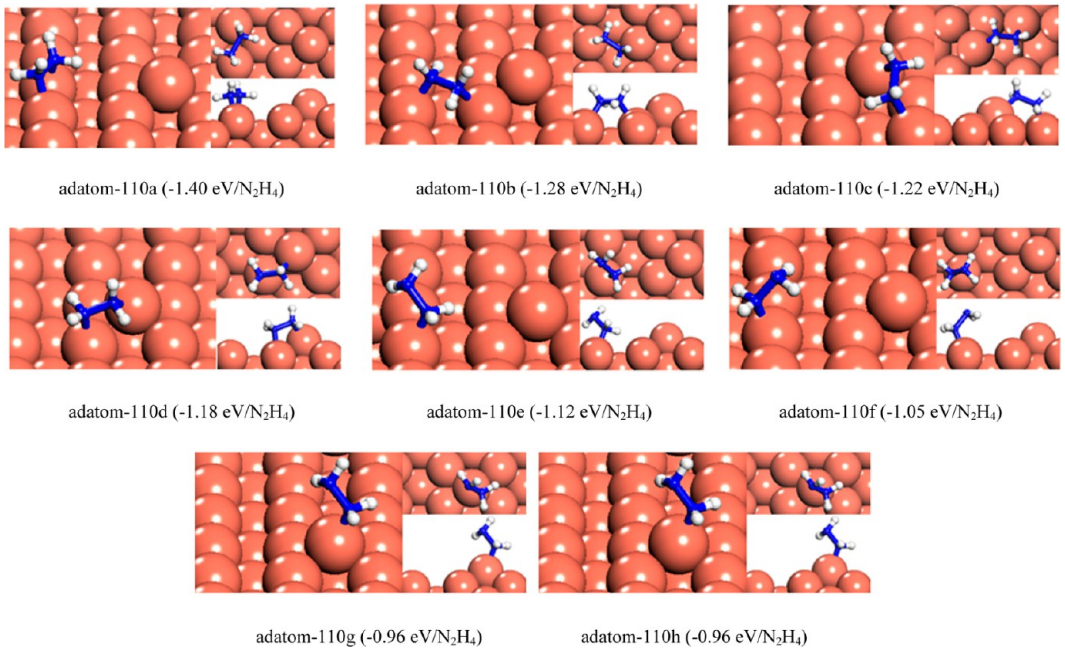

Figure 12. Lowest-energy configurations for adsorption of N_2H_4 on the adatom Cu (110) surface. (Adsorption energies are given in parentheses.)

Table 9. Geometries and Adsorption Energies (E_{ads}) of the Relaxed N_2H_4 Adsorbed Structures on the Adatom Cu(110) Surface[a]

label	geometry	E_{ads} (eV/N_2H_4)	N−Cu (Å)	N−Cu (Å)	N−N (Å)	Θ (deg)
adatom-110a	bridge-surface atoms	−1.40	2.09	2.10	1.45	0.30
adatom-110b	bridge-surface atoms	−1.28	2.13	2.17	1.45	1.20
adatom-110c	bridge-adatom-surface atom	−1.22	**2.19**	2.16	1.46	22.41
adatom-110d	bridge-adatom-surface atom	−1.18	**2.12**	2.11	1.45	21.94
adatom-110e	gauche-atop-surface atom	−1.12	2.06	2.99	1.45	38.37
adatom-110f	trans-atop-surface atom	−1.05	2.03	3.04	1.47	50.73
adatom-110g	gauche-atop-adatom	−0.96	**2.05**	3.01	1.45	48.53
adatom-110h	trans-atop-adatom	−0.96	**2.02**	3.02	1.48	47.48

[a]Bold numbers indicate a nitrogen atom is bound to the adatom.

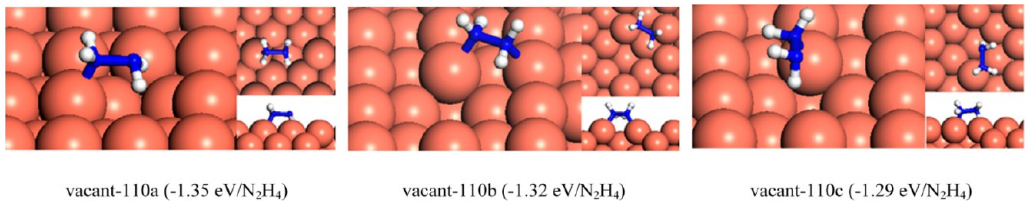

Figure 13. Lowest-energy configurations for adsorption of N_2H_4 on the Cu(110) vacancy surface. (Adsorption energies are given in parentheses.)

the adatom (Figure 12, adatom-110c) is preferred over bridging to the closest copper atom (Figure 12, adatom-110d).

Figure 12 also shows the adsorption structures where N_2H_4 adsorbs through a single nitrogen atom, atop either a surface copper atom (adatom-110e, f) or an adatom (adatom-110g, h). As Table 9 shows, binding to the top site is stronger than to the adatom. Adsorption of hydrazine in either gauche or trans conformation on the adatom releases 0.96 eV/N_2H_4, while adsorption of N_2H_4 on a surface copper atom in the gauche conformation is more favorable than in the trans conformation by 0.07 eV/N_2H_4.

We found that the bridging site between the adatom and a surface atom is the preferred position for the molecule on the (111) surface,[21] but in the strongest adsorption structures on the adatom (100) and (110) surfaces, hydrazine prefers to bridge between surface atoms without involving the adatom, because these surfaces already contain low-coordinated atoms in the defect-free planes.

3.4.4. Adsorption on the (110) Vacancy Surface. We found the strongest adsorption on the Cu(110) surface with vacancy, releasing an energy of 1.35 eV/N_2H_4, when the molecule in the trans conformation interacts through only one nitrogen with a surface atom next to the vacancy at a Cu−N distance of 2.02 Å (Figure 13, vacant-110a). The channels between rows next to the vacancy accommodate N_2H_4 very well, leading to strong binding to the surface. The lowest-energy structures are schematically shown in Figure 13, with geometric and energetic details summarized in Table 10.

We identified two other structures close in energy, where hydrazine bridges between two atoms next to the vacancy, with an adsorption energy of −1.32 eV/N_2H_4 (Figure 13, vacant-110b), similar to the molecule adsorbing on top of the atom next

dx.doi.org/10.1021/jp5078664 | J. Phys. Chem. C 2014, 118, 26103−26114

Table 10. Geometries and Adsorption Energies (E_{ads}) of the Relaxed N_2H_4 Adsorbed Structures on the Cu(110) Vacancy Surface[a]

label	geometry	E_{ads} (eV/N_2H_4)	N–Cu (Å)	N–Cu (Å)	N–N (Å)	Θ (deg)
vacant-110a	trans-atop	−1.35	2.02	**2.95**	1.48	0.7
vacant-110b	bridge	−1.32	2.13	2.16	1.45	1.1
vacant-110c	gauche-atop	−1.29	2.04	**2.96**	1.45	2.5

[a]Bold numbers indicate a nonbonding nitrogen atom.

to the vacancy in a gauche conformation (Figure 13, vacant-110c), $E_{ads} = -1.29$ eV/N_2H_4.

3.5. Morphology. The equilibrium morphology of a crystal is determined by the surface energies and the related growth rates of the various surfaces and provides a measure of the relative stabilities of the surfaces. Wulff's Theorem[42] states that a polar plot of surface energy versus orientation of normal vectors would give the crystal morphology based on the approach of Gibbs,[43] who proposed that under thermodynamic control the equilibrium form of a crystal should possess minimal total surface free energy for a given volume. Lattice dynamics simulations have shown that the contribution of the excess entropy term to the surface free energy is small compared to the enthalpy term, as the differences between the entropies of the bulk and the surface are small and, hence, for solid surfaces the surface energy is a close approximation of the surface free energy.[44] Thus, the surface energies can be assumed to determine the equilibrium morphology of the crystal. This approach has been employed in the calculation of the effect of surface adsorbates on the thermodynamic morphologies of many different materials, e.g. oxides, carbonates, phosphates and sulfides,[44−49] where good agreement was obtained with experiment. We have therefore used the same approach here to obtain the morphologies of the copper particles and investigate the effect of hydrazine adsorption on the expression of the different surfaces in the resulting morphologies. Wulff crystal morphologies were calculated from the surface energies of the perfect and defect-containing copper surfaces listed in Table 2. The calculated cuboctahedron morphology deriving from the surface energies of the perfect, adatom, and vacancy surfaces, represented in Figure 14a, shows that the (111) surface is highly prominent but that the (100) and (110) planes are also expressed. It also indicates that the introduction of point defects on the surfaces does not change the morphology. However, the addition of an extended defect, such as steps on the surfaces (Figure 14b), does affect the crystal shape; in the extreme case, where all surfaces are considered to contain high step densities, the (110) surface disappears from the Cu morphology due to its relatively high surface energy.

We have also obtained the morphology of Cu particles after adsorption of N_2H_4 on the surfaces, using eq 5

$$\gamma_r = \frac{E_{slab+N_2H_4} - [nE_{bulk} + E_{N_2H_4}]}{A} - \frac{E_{slab}^{unrelaxed} - nE_{bulk}}{2A} \quad (5)$$

Since the surface energies change as an effect of hydrazine adsorption, the morphology is altered. Due to a decrease in the surface energy, and therefore increase in the stability, of the (110) surface upon hydrazine adsorption, the particles' morphology shows an increase in (110) surface area (Figure 14c,d). We should note, however, that these results are based on the adsorption of only one N_2H_4 molecule on the Cu surfaces, whereas increasing the hydrazine coverage on the surfaces may conceivably lead to further expression of the (110) surface in the morphology. These results are in agreement with previous experiments which showed that N_2H_4 stabilizes the surfaces as a capping agent during Cu nanoparticle synthesis, thereby modifying the nanoparticles' shapes and sizes.[13]

3.6. Electronic Structure. We have obtained the electronic density of states (DOS) (Figure 15) to investigate if the electronic structures of the N p-orbitals of the two nitrogen atoms in hydrazine remain identical or become different upon adsorption, depending on how the N_2H_4 molecules interact with the surface, i.e., through both nitrogens or through only a single nitrogen atom. The symmetry of the bridging configurations on perfect-100 (Figure 15a) is shown by the identical electronic structure of the N p-orbitals. However, the local electronic density of states projections (LDOS) on the N p-band of the adatom-100 (Figure 15b) and vacant-110 (Figure 15c) surfaces show a shift to lower energies for the nitrogen atom closer to the surface. This shift can also be seen on the stepped (110) (Figure 15d) for the N atom interacting with the Cu atom on the step edge.

In order to analyze the observed N p-band shift in the atop hydrazine adsorption structures and identify any changes in the charges of the adsorbed molecule compared to hydrazine in the gas phase, we have carried out Bader[50] charge analyses implemented in the Henkelman algorithm.[51] The charge analysis shows that, on those structures where hydrazine interacts through only one atom to the surface, the N atom interacting with the surface is more negatively charged (-0.81 e^-) compared with the noninteracting N (0.72 e^-), whereas the charge of the N atom of hydrazine in the gas phase is -0.73 e^-. This charge distribution is in agreement with the DOS, where there is a larger shift in energy of the p-bands of the interacting N atom, whereas in the bridging configurations both N atoms of hydrazine have

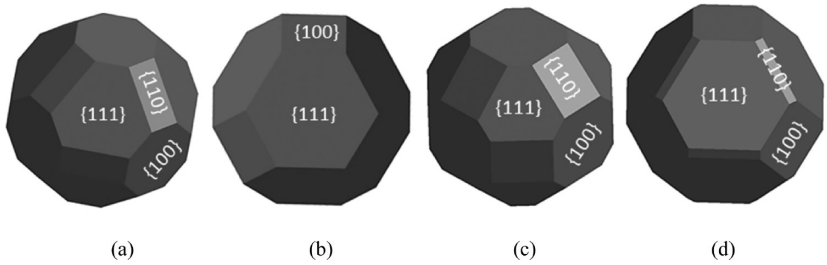

Figure 14. Calculated crystal morphology of copper before hydrazine adsorption: (a) perfect, adatom, and vacancy, (b) step crystals; and after hydrazine adsorption: (c) perfect, adatom, and vacancy, (d) step crystals.

dx.doi.org/10.1021/jp5078664 | J. Phys. Chem. C 2014, 118, 26103−26114

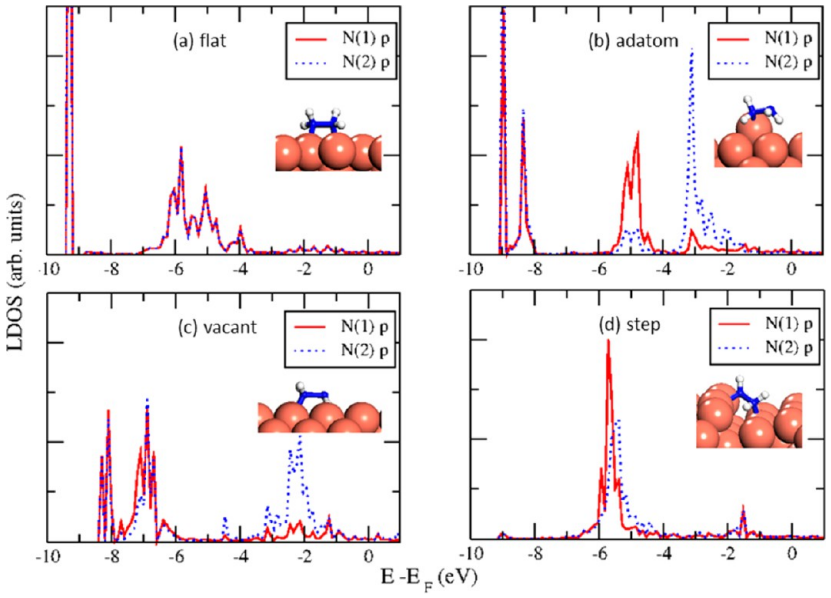

Figure 15. Site-projected electronic LDOS of the lowest-energy adsorbed structures on (a) perfect (100), (b) adatom (100), (c) vacant (110), and (d) stepped (110) surfaces for nitrogen p-band. N(1) is the nitrogen closest to the surface and N(2) is the second nitrogen atom of N_2H_4.

practically the same charge (−0.78 e^-). On all investigated Cu surfaces, the resulting net charge transfer between the N_2H_4 and surface is very small (less than 0.1 e^-/N), where the observed distortion of the molecule indicates electronic rearrangement upon adsorption, suggesting a chemical interaction between the molecule and the surface and covalent character of the Cu−N bond.

3.7. Coordination Number. It is clear that the hydrazine molecule adsorbs more strongly on the perfect (110) surface compared to the perfect (100) and (111) Cu surfaces. The Cu atoms in the perfect (110) surface have a coordination number (CN) of 7, while the perfect (100) surface atoms are 8-fold coordinated, showing a weaker N_2H_4 adsorption, with the weakest adsorption taking place on the perfect (111) surface where the CN is 9; This trend is in line with other theoretical studies.[17,18] Although the low-coordinated atoms on the perfect (110) allow the molecule to bind strongly to the surface, the introduction of defects can also provide sites for strong adsorption on the more stable (111) and (100) surfaces.

In order to clarify the effect of CN on the adsorption energy, we have analyzed the adsorption energy per Cu−N bond with respect to the coordination number of the interacting Cu atoms. Within this approximation, where hydrazine interacts through both N atoms to surface Cu atoms with the same CN, because the N atoms of the hydrazine molecule in that case have the same LDOS and charge, the binding energy per Cu−N bond is obtained by halving their respective total adsorption energies. In the structures where the two N atoms bind to surface Cu atoms with different CNs and where one Cu has the same CN as on flat surface, we assume that the energy per Cu−N bond is obtained by the difference between the total adsorption energy of hydrazine at the surface and the adsorption energy per Cu−N bond on the flat surface. However, the calculation of the adsorption energies per interacting N atom is difficult on the (100) adatom and vacancy-containing surfaces, where hydrazine interacts through a single N atom to the surface, because, in principle, we cannot calculate the contribution of the non-bonding N atom to the total adsorption energy. On these surfaces, we have therefore used the second lowest-energy structures, where hydrazine interacts through both N atoms, which enables us to calculate the adsorption energy per Cu−N bond for all surfaces. A plot of the adsorption energy per Cu−N bond as a function of the CN of the interacting Cu is shown in Figure 16a, from which it is evident that creating defects with lower CN sites leads to stronger binding. Interestingly, the same CN leads to practically the same E_{ads} on different surfaces, to within 0.1 eV, independent of the adsorption site.

It has been shown that the d-band center model of chemisorption, developed by Hammer and Nørskov,[52,53] can predict the trend in adsorption energies of various adsorbates on metal surfaces. In general, the closest the energy of the d-band center of the site to the Fermi level, the stronger the binding of the adsorbate to the surface. In the present study, we have found a trend of d-band center as a function of CN of interacting Cu surface atom, presented in Figure 16b. The linear-trend line indicaties a direct relationship between CN and the d-band center of the metal atom. This linear relationship allows us to predict future adsorption affinities based on the CN alone, without the need to calculate the electronic structure of the metallic surface projected on a particular interacting site.

4. CONCLUSIONS

We have used DFT-D2 calculations to investigate the adsorption of hydrazine on perfect and defect-containing (100) and (110) surfaces of copper and compared the results with those for the (111) surfaces from earlier work.[21] The strength of the adsorption on the perfect surfaces is related to their stability and therefore follows the trend (110) > (100) > (111). The creation of defects in the form of steps, Cu-adatoms, and vacancies provides lower-coordinated Cu sites, allowing stronger hydrazine adsorption. The presence of an extended edge of low-coordinated surface atoms in the form of a step on the (110) surface results in the strongest binding of hydrazine to any of the copper surfaces. The effect of the introduction of defects is more important on the more stable surfaces, i.e., while the presence of a step on the (111) surface almost doubles the strength of adsorption compared to the planar surface, the increase in binding strength to the stepped (100) and (110) surfaces is only

dx.doi.org/10.1021/jp5078664 | J. Phys. Chem. C 2014, 118, 26103−26114

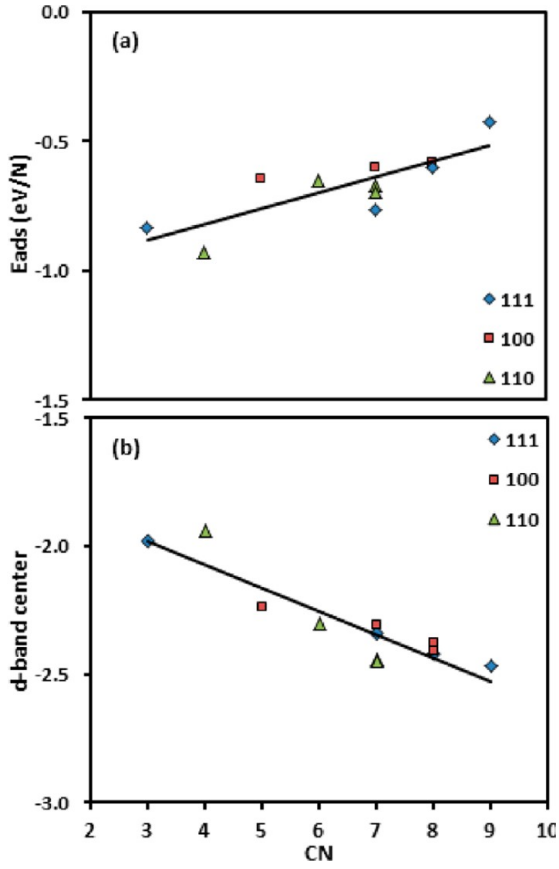

Figure 16. (a) Adsorption energy per N interaction, (b) d-band center of interacting Cu atoms as a function of coordination number (CN) of interacting Cu atoms, for the lowest-energy adsorption structures on the perfect and defective Cu(100), (110), and (111) surfaces, except on the adatom (100) and vacancy surfaces, where we used the second lowest-energy adsorption structures (see text). The linear trend-lines in the plots fit the equation (a) $y = -0.09x - 1.71$, $R^2 = 0.84$ and (b) $y = 0.0605x - 1.0648$, $R^2 = 0.68$.

1.10 and 1.19 times that of the binding on the flat (100) and (110) surfaces, respectively. However, adsorption of hydrazine to the stepped (110) surface remains the strongest.

The preferred geometry for hydrazine adsorption on any of the perfect and defective (110) and (100) surfaces is through the molecule bridging two surface copper atoms through both N atoms, except on the (100) adatom, and the (100) and (110) vacancy-containing surfaces, where a structure with only one N on a top site is preferred, with the hydrazine in gauche and trans conformations, respectively. A shift occurs of the N p-orbital toward lower energies for those N atoms of hydrazine that are closer to the surface, where they gain more charge.

The thermodynamic morphology of the Cu nanocrystal can be affected by the presence of defects and further changes upon hydrazine adsorption. A linear trend for hydrazine adsorption as a function of CN, as well as for the site d-band electronic structure, indicates that lower CN atoms provide sites with d-band centers closer to the Fermi level, which allows stronger binding. The linear trend lines offer a predictive route to match adsorption strength to CN and d-band center.

AUTHOR INFORMATION

Corresponding Author

*Tel.: +44 2076791015. Fax: +44 2076797463. E-mail: n.h.deleeuw@ucl.ac.uk.

Notes

The authors declare no competing financial interest.

ACKNOWLEDGMENTS

S.S.T. acknowledges University College London and the UCL Industrial Doctorate Centre in Molecular Modelling and Material Science for an Overseas Research Scholarship. N.H.d.L. acknowledges the Royal Society for an Industry Fellowship and A.R. is grateful to the Ramsay Memorial Trust and University College London for the award of a Ramsay Fellowship. Via our membership of the U.K.'s HPC Materials Chemistry Consortium, which is funded by EPSRC (EP/L000202), this work made use of the facilities of HECToR and ARCHER, the U.K.'s national high-performance computing service, which is funded by the Office of Science and Technology through EPSRC's High End Computing Programme, as well as the UCL Legion High Performance Computing facility (Legion@UCL), and associated support services, in the completion of this work.

REFERENCES

(1) Fahlman, B. D. *Materials Chemistry*; Springer: Berlin, 2007.

(2) Heath, J. R. Nanoscale Materials. *Acc. Chem. Res.* **1999**, *32*, 388−388.

(3) Matsui, I. Nanoparticles for Electronic Device Applications: A Brief Review. *J. Chem. Eng. Jpn.* **2005**, *38*, 535−546.

(4) Liu, W. T. Nanoparticles and Their Biological and Environmental Applications. *J. Biosci. Bioeng.* **2006**, *102*, 1−7.

(5) Lisiecki, I.; Pileni, M. P. Synthesis of Copper Metallic Clusters Using Reverse Micelles as Microreactors. *J. Am. Chem. Soc.* **1993**, *115*, 3887−3896.

(6) Salzemann, C.; Lisiecki, I.; Brioude, A.; Urban, J.; Pileni, M. P. Collections of Copper Nanocrystals Characterized by Different Sizes and Shapes: Optical Response of These Nanoobjects. *J. Phys. Chem. B* **2004**, *108*, 13242−13248.

(7) Germain, V.; Brioude, A.; Ingert, D.; Pileni, M. P. Silver Nanodisks: Size Selection Via Centrifugation and Optical Properties. *J. Chem. Phys.* **2005**, *122*.

(8) Kooij, E. S.; Poelsema, B. Shape and Size Effects in the Optical Properties of Metallic Nanorods. *Phys. Chem. Chem. Phys.* **2006**, *8*, 3349−3357.

(9) Salzemann, C.; Brioude, A.; Pileni, M. P. Tuning of Copper Nanocrystals Optical Properties with Their Shapes. *J. Phys. Chem. B* **2006**, *110*, 7208−7212.

(10) El-Sayed, M. A. Small Is Different: Shape-, Size-, and Composition-Dependent Properties of Some Colloidal Semiconductor Nanocrystals. *Acc. Chem. Res.* **2004**, *37*, 326−333.

(11) Filankembo, A.; Giorgio, S.; Lisiecki, I.; Pileni, M. P. Is the Anion the Major Parameter in the Shape Control of Nanocrystals? *J. Phys. Chem. B* **2003**, *107*, 7492−7500.

(12) Salzemann, C.; Lisiecki, L.; Urban, J.; Pileni, M. P. Anisotropic Copper Nanocrystals Synthesized in a Supersaturated Medium: Nanocrystal Growth. *Langmuir* **2004**, *20*, 11772−11777.

(13) Lisiecki, I. Size, Shape, and Structural Control of Metallic Nanocrystals. *J. Phys. Chem. B* **2005**, *109*, 12231−12244.

(14) Andrew, M. R.; Gressler, W. J.; Johnson, J. K.; Short, R. T.; Williams, K. R. Engineering Aspects of Hydrazine-Air Fuel-Cell Power Systems. *J. Appl. Electrochem.* **1972**, *2*, 327.

(15) Granot, E.; Filanovsky, B.; Presman, I.; Kuras, I.; Patolsky, F. Hydrazine/Air Direct-Liquid Fuel Cell Based on Nanostructured Copper Anodes. *J. Power Sources* **2012**, *204*, 116−121.

(16) Yamada, K.; Asazawa, K.; Yasuda, K.; Ioroi, T.; Tanaka, H.; Miyazaki, Y.; Kobayashi, T. Investigation of Pem Type Direct Hydrazine Fuel Cell. *J. Power Sources* **2003**, *115*, 236−242.
(17) Daff, T. D.; Costa, D.; Lisiecki, I.; de Leeuw, N. H. Density Functional Theory Calculations of the Interaction of Hydrazine with Low-Index Copper Surfaces. *J. Phys. Chem. C* **2009**, *113*, 15714−15722.
(18) Daff, T. D.; de Leeuw, N. H. A Density Functional Theory Investigation of the Molecular and Dissociative Adsorption of Hydrazine on Defective Copper Surfaces. *J. Mater. Chem.* **2012**, *22*, 23210−23220.
(19) Daff, T. D.; Saadoune, I.; Lisiecki, I.; de Leeuw, N. H. Computer Simulations of the Effect of Atomic Structure and Coordination on the Stabilities and Melting Behaviour of Copper Surfaces and Nano-Particles. *Surf. Sci.* **2009**, *603*, 445−454.
(20) Daff, T. D.; de Leeuw, N. H. Ab Initio Molecular Dynamics Simulations of the Cooperative Adsorption of Hydrazine and Water on Copper Surfaces: Implications for Shape Control of Nanoparticles. *Chem. Mater.* **2011**, *23*, 2718−2728.
(21) Tafreshi, S. S.; Roldan, A.; Dzade, N. Y.; de Leeuw, N. H. Adsorption of Hydrazine on the Perfect and Defective Copper (111) Surface: A Dispersion-Corrected Dft Study. *Surf. Sci.* **2014**, *622*, 1−8.
(22) Tang, Q. L.; Chen, Z. X. Density Functional Slab Model Studies of Water Adsorption on Flat and Stepped Cu Surfaces. *Surf. Sci.* **2007**, *601*, 954−964.
(23) Grimme, S. Accurate Description of Van Der Waals Complexes by Density Functional Theory Including Empirical Corrections. *J. Comput. Chem.* **2004**, *25*, 1463−1473.
(24) Grimme, S. Semiempirical Gga-Type Density Functional Constructed with a Long-Range Dispersion Correction. *J. Comput. Chem.* **2006**, *27*, 1787−1799.
(25) Kresse, G.; Furthmuller, J. Efficient Iterative Schemes for Ab Initio Total-Energy Calculations Using a Plane-Wave Basis Set. *Phys. Rev. B* **1996**, *54*, 11169−11186.
(26) Kresse, G.; Furthmuller, J. Efficiency of Ab-Initio Total Energy Calculations for Metals and Semiconductors Using a Plane-Wave Basis Set. *Comp. Mater. Sci.* **1996**, *6*, 15−50.
(27) Kresse, G.; Hafner, J. Abinitio Molecular-Dynamics for Liquid-Metals. *Phys. Rev. B* **1993**, *47*, 558−561.
(28) Kresse, G.; Hafner, J. Ab-Initio Molecular-Dynamics Simulation of the Liquid-Metal Amorphous-Semiconductor Transition in Germanium. *Phys. Rev. B* **1994**, *49*, 14251−14269.
(29) Kresse, G.; Joubert, D. From Ultrasoft Pseudopotentials to the Projector Augmented-Wave Method. *Phys. Rev. B* **1999**, *59*, 1758−1775.
(30) Blochl, P. E. Projector Augmented-Wave Method. *Phys. Rev. B* **1994**, *50*, 17953−17979.
(31) Perdew, J. P.; Burke, K.; Ernzerhof, M. Generalized Gradient Approximation Made Simple. *Phys. Rev. Lett.* **1996**, *77*, 3865−3868.
(32) Monkhorst, H. J.; Pack, J. D. Special Points for Brillouin-Zone Integrations. *Phys. Rev. B* **1976**, *13*, 5188−5192.
(33) Strauman.Me; Yu, L. S. Lattice Parameters, Densities, Expansion Coefficients and Perfection of Structure of Cu and of Cu-in Alpha Phase. *Acta Cryst. a-Cryst.* **1969**, *A 25*, 676−&.
(34) de Leeuw, N. H.; Parker, S. C.; Catlow, C. R. A.; Price, G. D. Proton-Containing Defects at Forsterite {010} Tilt Grain Boundaries and Stepped Surfaces. *Am. Mineral.* **2000**, *85*, 1143−1154.
(35) de Leeuw, N. H.; Nelson, C. J. A Computer Modeling Study of Perfect and Defective Silver (111) Surfaces. *J. Phys. Chem. B* **2003**, *107*, 3528−3534.
(36) de Leeuw, N. H.; Nelson, C. J.; Catlow, C. R. A.; Sautet, P.; Dong, W. Density-Functional Theory Calculations of the Adsorption of Cl at Perfect and Defective Ag(111) Surfaces. *Phys. Rev. B* **2004**, *69*.
(37) Yildirim, H.; Kara, A.; Durukanoglu, S.; Rahman, T. S. Calculated Pre-Exponential Factors and Energetics for Adatom Hopping on Terraces and Steps of Cu(100) and Cu(110). *Surf. Sci.* **2006**, *600*, 484−492.
(38) Karimi, M.; Tomkowski, T.; Vidali, G.; Biham, O. Diffusion of Cn on Cu Surfaces. *Phys. Rev. B* **1995**, *52*, 5364−5374.
(39) Eremeev, S. V.; Lipnitskii, A. G.; Potekaev, A. I.; Chulkov, E. V. Diffusion Activation Energy of Point Defects at the Surfaces of Fcc Metals. *Phys. Low-Dimens. Str.* **1997**, *3*−*4*, 127−133.
(40) Skriver, H. L.; Rosengaard, N. M. Surface Energy and Work Function of Elemental Metals. *Phys. Rev. B* **1992**, *46*, 7157−7168.
(41) Vitos, L.; Ruban, A. V.; Skriver, H. L.; Kollar, J. The Surface Energy of Metals. *Surf. Sci.* **1998**, *411*, 186−202.
(42) Wulff, G. On the Question of Speed of Growth and Dissolution of Crystal Surfaces. *Z. Krystallogr. Miner.* **1901**, *34*, 449−530.
(43) Gibbs, J. W. *In Collected Works*; Longman: New York, 1928.
(44) Mkhonto, D.; de Leeuw, N. H. A Computer Modelling Study of the Effect of Water on the Surface Structure and Morphology of Fluorapatite: Introducing a Ca-10(Po4)(6)F-2 Potential Model. *J. Mater. Chem.* **2002**, *12*, 2633−2642.
(45) de Leeuw, N. H.; Parker, S. C. Effect of Chemisorption and Physisorption of Water on the Surface Structure and Stability of Alpha-Alumina. *J. Am. Ceram. Soc.* **1999**, *82*, 3209−3216.
(46) de Leeuw, N. H.; Cooper, T. G. Surface Simulation Studies of the Hydration of White Rust Fe(Oh)(2), Goethite Alpha-Feo(Oh) and Hematite Alpha-Fe(2)O(3). *Geochim Cosmochim Ac* **2007**, *71*, 1655−1673.
(47) Santos-Carballal, D.; Roldan, A.; Grau-Crespo, R.; de Leeuw, N. H. A Dft Study of the Structures, Stabilities and Redox Behaviour of the Major Surfaces of Magnetite Fe3o4. *Phys. Chem. Chem. Phys.* **2014**, *16*, 21082−21097.
(48) Devey, A. J.; Grau-Crespo, R.; de Leeuw, N. H. Combined Density Functional Theory and Interatomic Potential Study of the Bulk and Surface Structures and Properties of the Iron Sulfide Mackinawite (Fes). *J. Phys. Chem. C* **2008**, *112*, 10960−10967.
(49) de Leeuw, N. H.; Parker, S. C. Surface Structure and Morphology of Calcium Carbonate Polymorphs Calcite, Aragonite, and Vaterite: An Atomistic Approach. *J. Phys. Chem. B* **1998**, *102*, 2914−2922.
(50) Bader, R. F. W.; Carroll, M. T.; Cheeseman, J. R.; Chang, C. Properties of Atoms in Molecules - Atomic Volumes. *J. Am. Chem. Soc.* **1987**, *109*, 7968−7979.
(51) Henkelman, G.; Arnaldsson, A.; Jonsson, H. A Fast and Robust Algorithm for Bader Decomposition of Charge Density. *Comp. Mater. Sci.* **2006**, *36*, 354−360.
(52) Hammer, B.; Norskov, J. K. Electronic Factors Determining the Reactivity of Metal Surfaces. *Surf. Sci.* **1995**, *343*, 211−220.
(53) Greeley, J.; Norskov, J. K.; Mavrikakis, M. Electronic Structure and Catalysis on Metal Surfaces. *Annu. Rev. Phys. Chem.* **2002**, *53*, 319−348.